

# Nuclear Diagnostics of ICF

*N. Izumi, R.A. Lerche, M.J. Moran, T.W. Phillips, T.C. Sangster, G.J. Schmid, M.A. Stoyer, L. Disdier, J.L. Bourgade, A. Rouyer, R.K. Fisher, R.R. Berggren, S.E. Caldwell, J.R. Faulkner, J.M. Mack, J.A. Oertel, C.S. Young, V.Y. Glebov, P.A. Jaanimagi, D.D. Meyerhofer, J.M. Soures, C. Stoeckl, J.A. Frenje, C.K. Li, R.D. Petrasso*

This article was submitted to  
6<sup>th</sup> International Conference on Advanced Diagnostics for Magnetic  
and Inertial Fusion, Villa Monastero, Varenna, Italy, September 3-7,  
2001

U.S. Department of Energy

Lawrence  
Livermore  
National  
Laboratory

**October 18, 2001**

## DISCLAIMER

This document was prepared as an account of work sponsored by an agency of the United States Government. Neither the United States Government nor the University of California nor any of their employees, makes any warranty, express or implied, or assumes any legal liability or responsibility for the accuracy, completeness, or usefulness of any information, apparatus, product, or process disclosed, or represents that its use would not infringe privately owned rights. Reference herein to any specific commercial product, process, or service by trade name, trademark, manufacturer, or otherwise, does not necessarily constitute or imply its endorsement, recommendation, or favoring by the United States Government or the University of California. The views and opinions of authors expressed herein do not necessarily state or reflect those of the United States Government or the University of California, and shall not be used for advertising or product endorsement purposes.

This is a preprint of a paper intended for publication in a journal or proceedings. Since changes may be made before publication, this preprint is made available with the understanding that it will not be cited or reproduced without the permission of the author.

This report has been reproduced directly from the best available copy.

Available electronically at <http://www.doe.gov/bridge>

Available for a processing fee to U.S. Department of Energy  
and its contractors in paper from  
U.S. Department of Energy  
Office of Scientific and Technical Information  
P.O. Box 62  
Oak Ridge, TN 37831-0062  
Telephone: (865) 576-8401  
Facsimile: (865) 576-5728  
E-mail: [reports@adonis.osti.gov](mailto:reports@adonis.osti.gov)

Available for the sale to the public from  
U.S. Department of Commerce  
National Technical Information Service  
5285 Port Royal Road  
Springfield, VA 22161  
Telephone: (800) 553-6847  
Facsimile: (703) 605-6900  
E-mail: [orders@ntis.fedworld.gov](mailto:orders@ntis.fedworld.gov)  
Online ordering: <http://www.ntis.gov/ordering.htm>

OR

Lawrence Livermore National Laboratory  
Technical Information Department's Digital Library  
<http://www.llnl.gov/tid/Library.html>

## NUCLEAR DIAGNOSTICS OF ICF

N. Izumi, R.A. Lerche, M.J. Moran, T.W. Phillips, T.C. Sangster, G.J. Schmid, M.A. Stoyer, L. Disdier, J. L. Bourgade, A. Rouyer, R. K. Fisher, R. R. Berggren, S. E. Caldwell, J. R. Faulkner, J. M. Mack, J. A. Oertel, C. S. Young, V. Yu. Glebov, P. A. Jaanimagi, D. D. Meyerhofer, J. M. Soures, C. Stoeckl, J. A. Frenje, C. K. Li, and R. D. Petrasso

### 1. INTRODUCTION

In inertial confinement fusion (ICF), a high temperature and high density plasma is produced by the spherical implosion of a small capsule<sup>1</sup>. A spherical target capsule is irradiated uniformly by a laser beam (direct irradiation) or x-rays from a high Z enclosure (hohlraum) that is irradiated by laser or ion beams (indirect irradiation). Then high-pressure ablation of the surface causes the fuel to be accelerated inward. Thermonuclear fusion reactions begin in the center region of the capsule as it is heated to sufficient temperature (10 keV) by the converging shocks (hot spot formation). During the stagnation of the imploded shell, the fuel in the shell region is compressed to high density ( $\sim 10^3$  times solid density in fuel region). When these conditions are established, energy released by the initial nuclear reactions in center "hot-spot" region can heat up the cold "fuel" region and cause ignition.

We are developing advanced nuclear diagnostics for imploding plasmas of the ignition campaign on the National Ignition Facility (NIF). The NIF is a 1.8MJ, 192-beam glass laser system that is under construction at Lawrence Livermore National

---

<sup>1</sup> N. Izumi, R.A. Lerche, M.J. Moran, T.W. Phillips, G.J. Schmid, M.A. Stoyer, Lawrence Livermore National Laboratory, P. O. Box 808 Livermore CA, 94550; L. Disdier, J. L. Bourgade, A. Rouyer, Commissariat à l'Energie Atomique, Bruyères-le-Châtel, France; R. K. Fisher, General Atomics, San Diego, CA 92121; R. R. Berggren, S. E. Caldwell, J. R. Faulkner, J. M. Mack, J. A. Oertel, C. S. Young, Los Alamos National Laboratory, Los Alamos, New Mexico 87545; T.C. Sangster, V. Yu. Glebov, P. A. Jaanimagi, D. D. Meyerhofer, J. M. Soures, C. Stoeckl, Laboratory for Laser Energetics, University of Rochester, Rochester, New York 14623; J. A. Frenje, C. K. Li, and R. D. Petrasso, Plasma Science and Fusion Center, Massachusetts Institute of Technology, Cambridge, Massachusetts 02139

Laboratory<sup>1</sup>. One objective of the NIF is to demonstrate ignition and gain in an inertial confinement fusion plasma.

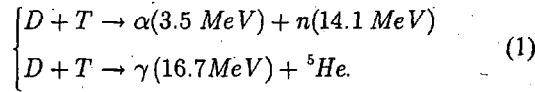
Extreme physical conditions characterize the imploded plasmas on the NIF. First, the thickness of the plasma, expressed by areal density (plasma density times radius), is large, up to  $\sim 1 \text{ g/cm}^2$ . Highly penetrating probes such as energetic neutrons, hard x-rays, or  $\gamma$  rays are required to see deep inside the plasma. Second, the implosion time is quite short. The implosion process takes  $\sim 20 \text{ ns}$  and the duration of the fusion reaction is on the order of 100 picoseconds. To observe the time history of the nuclear reactions, time resolution better than 10 ps is required. Third, the size of the imploded plasma is quite small ( $\sim 100 \text{ }\mu\text{m}$ ). To see the shape of burning region, a spatial resolution of  $\sim 5 \text{ }\mu\text{m}$  is required for imaging systems. Fourth, the diagnostics operate in a harsh background. In implosion experiments, strong bursts of electromagnetic pulses, x-rays, neutrons, and neutron-induced radioactivity are produced. Therefore the diagnostics have to be designed to survive in these backgrounds. In addition, to prevent materials ablated from diagnostic components close to the target from being deposited on the laser optics, these components will be excluded from a zone around the target with a radius in the range of 0.5 m to 5m. This exclusion zone has a large impact on diagnostic design.

## 2. BASIC NUCLEAR REACTIONS IN ICF PLASMAS

This section reviews the fundamental nuclear reaction in the fuel plasma. For ignition experiments, the target capsules are cryogenic and consist of an ablator layer, a solid deuterium-tritium (DT) fuel, and a central DT gas region.

### 2.1. Primary reactions in DT capsule

In the DT filled fuel, the primary reactions that are important for diagnostics\* are<sup>1</sup>



Due to its large cross section, the  $t(d,n)\alpha$  reaction is dominant in DT filled capsule. The spectral width of the DT neutrons, (full width at half maximum)  $\Delta E$  (keV) is given<sup>2</sup> as a function of ion temperature  $T_i$  (keV), by  $\Delta E = 177 \times T_i^{0.5}$ . This relation is used for the ion temperature measurement. However for a neutron emission history measurement, the neutron velocity distribution due to the thermal broadening degrades the temporal resolution at exclusion zone distances. Instead of the neutrons, the  $\gamma$  ray branch is more useful for a burn history measurement. The branching ratio of this reaction is  $5 \times 10^{-5}$  (ref. 3). A burn history measurement using 16.7-MeV  $\gamma$ -rays will be discussed.

### 2.2. Tertiary reaction in DT fuel

---

\*  $d(d,n){}^3\text{He}$ ,  $d(d,p)t$ ,  $t(t,2n)\alpha$  are also primary reactions in DT filled target.

Tertiary reactions in DT filled capsules will be used for an areal density measurement<sup>4</sup>. It is also possible to use tertiary protons for an areal density measurement via <sup>3</sup>He seeding in DT fuel. A small fraction of primary neutrons recoil from ions in the fuel,

$$\begin{cases} n(14.1 \text{ MeV}) + D \rightarrow n' + D^* (< 12.5 \text{ MeV}) \\ n(14.1 \text{ MeV}) + T \rightarrow n' + T^* (< 10.6 \text{ MeV}) \\ \text{With } ^3\text{He seeding, } n(14.1 \text{ MeV}) + ^3\text{He} \rightarrow n' + ^3\text{He}^* (< 10.6 \text{ MeV}). \end{cases} \quad (2)$$

The probability of these ion recoils is proportional to the areal density of the target ions in the capsule. (Areal density measurement using scattered DT primary neutrons is also being developed<sup>6,7</sup>.) These recoiling energetic ions cause tertiary reactions,

$$\begin{cases} D^* (< 12.5 \text{ MeV}) + T \rightarrow \alpha + n(12 - 30 \text{ MeV}) \\ T^* (< 10.6 \text{ MeV}) + D \rightarrow \alpha + n(9.2 - 28.1 \text{ MeV}). \end{cases} \quad (3)$$

With <sup>3</sup>He seeded in the initial DT fuel, the ion recoils produce tertiary protons by

$$\begin{cases} D^* (< 12.5 \text{ MeV}) + ^3\text{He} \rightarrow \alpha + p(12.5 - 30.8 \text{ MeV}) \\ ^3\text{He}^* (< 10.6 \text{ MeV}) + D \rightarrow \alpha + p(9.7 - 28.9 \text{ MeV}). \end{cases} \quad (4)$$

When the areal density of the fuel is small and the energy loss of the recoiling energetic ions (D, T, <sup>3</sup>He) is negligible, the production ratio of tertiary neutrons to primary neutrons is proportional to the square of the areal density. As the energy loss becomes significant, the tertiary neutron production increases more slowly with areal density.

### 2.3. Primary neutron in D<sub>2</sub> fuel

For various pre-ignition experiments such as implosion symmetry studies, deuterium filled capsules will be used. In deuterium filled fuel, the primary reactions are,

$$\begin{cases} D + D \rightarrow n(2.45 \text{ MeV}) + ^3\text{He}(0.82 \text{ MeV}) \\ D + D \rightarrow p(3.02 \text{ MeV}) + T(1.01 \text{ MeV}). \end{cases} \quad (5)$$

The expression in this case for thermal broadening of the neutron spectrum  $\Delta E(\text{keV})$  is  $\Delta E = 82.5 \times T_i^{0.5}$  (ref. 2). This relation is again useful for ion temperature measurement.

### 2.4. Secondary reaction in D<sub>2</sub> fuel

Energetic <sup>3</sup>He and T cause secondary reactions in the fuel<sup>8</sup>,

$$\begin{cases} {}^3\text{He}^* (< 1.01 \text{ MeV}) + D \rightarrow \alpha + p(12.5 - 17.4 \text{ MeV}) \\ T^* (< 0.82 \text{ MeV}) + D \rightarrow \alpha + n(11.8 - 17.1 \text{ MeV}) \end{cases} \quad (6)$$

When the energy loss of the energetic particles ( ${}^3\text{He}$  and  $T$ ) is negligible, the ratio of secondary to primary reaction product is proportional to the fuel areal density. Since the cross-sections for these reactions are functions of particle energy, the yield ratio of secondaries to primaries diverges from proportionality with increasing particle energy loss<sup>5</sup>. For the high areal densities expected of NIF capsules ( $\sim 1 \text{ g/cm}^2$ ), these particles are stopped in the fuel and the secondary to primary ratio is a measure of the ion range.

### 2.5. Scattered primary neutrons from $D_2$ filled capsule

The 2.45 MeV primary neutrons (Eq. 5) lose energy by elastic scattering in the target. The areal density  $\rho_D R$  of the deuterium plasma can be determined from the intensity ratio of lower energy (0.27-0.6 MeV) to primary neutrons (2.3-2.7 MeV). The areal density of deuterons can be determined from

$$\rho_D R \sim 6.0 \text{ g} \cdot \text{cm}^{-2} \times \frac{Y_n(0.27 - 0.6 \text{ MeV})}{Y_n(2.3 - 2.7 \text{ MeV})} \quad (7)$$

This relation (Eq. 7) saturates at higher areal densities. Allowing 15% divergence from linear relation, this technique is applicable up to  $\rho_D R = 3 \text{ g/cm}^2$ .

### 2.6. Scattered secondary neutrons from $D_2$ filled capsule

Secondary neutrons lose energy via  $d(n, \text{elastic})$  and  $d(n, 2n)p$  reactions in the target. The areal density  $\rho_D R$  of the deuterium plasma can be determined from the ratio of lower energy scattered neutrons (4-10 MeV) to the secondaries (12-17 MeV) as follows<sup>9</sup>,

$$\rho_D R \sim 9.2 \cdot \text{g} \cdot \text{cm}^{-2} \times \frac{Y_n(4 - 10 \text{ MeV})}{Y_n(12 - 17 \text{ MeV})} \quad (8)$$

This technique is applicable for a full scale NIF DD surrogate capsule.

## 3. CORE DIAGNOSTICS

Core diagnostics are defined as a group of basic diagnostic instruments, which have been used at NOVA, OMEGA and other large laser fusion facilities. The applicability and reliability of these diagnostics have already confirmed experimentally and require minimal R&D for application to NIF. In this category<sup>10</sup> the following diagnostics are included: (1) Primary and secondary neutron yield measurements with nuclear activation, (2) Neutron yield, ion temperature, and nuclear emission time measurements with current

mode scintillation detectors, (3) Areal density measurement via secondary and tertiary neutrons using a single-hit neutron detector array, and (4) Areal density measurements with a target activation technique using debris collection.

#### 4. ADVANCED NUCLEAR DIAGNOSTICS

The expected increase of nuclear reaction yields on the NIF will make it possible to utilize nuclear reactions with low cross sections for advanced diagnostics. In this section, recent progresses on the development of these advanced diagnostics are reported.

##### 4.1 Areal density measurement

The areal density of the imploded plasma is a crucial parameter that characterizes the performance of the implosion. The areal density of the hotspot  $\rho R_{HS} > 0.3 \text{ g/cm}^2$  is a necessary condition for ignition. The burn efficiency is proportional to the areal density of the fuel region. As discussed in a previous section, the diagnostic methods of areal density are based on the observation of the reactions of thermonuclear products with fuel ions. For DT capsules, neutrons or protons produced by tertiary reactions, or scattered primary neutrons will be used for areal density measurements. For  $D_2$  filled fuel, observations of the scattering by fuel ions of secondary or primary neutrons can be employed. To observe these neutrons, the detector must have a large dynamic range and operate in this harsh background environment. In a time-of-flight system, a strong burst of direct primary neutrons hits the detector before the scattered neutrons arrive at the detector. In order to detect the faint scattered signal after the primary burst, the detector must be able to recover quickly. The neutrons scattered by "non-target materials" (mainly vacuum chamber wall) cause background. There are two different ways to reduce the background due to "non-target" scattering. (1) Using a fast response detector within the target chamber and completing all measurements before the primary neutrons hit the chamber wall. (2) Using a sensitive detector outside the chamber and reducing the background with collimation. With these concepts, we are developing both the CVD diamond detector and the lithium-glass scintillation fiber detector.

##### 4.1.1. CVD diamond detector for short path operation:

At present we are developing a large area diamond detector to be used in current mode as a neutron TOF detector for a scattered secondary neutron measurement<sup>11</sup>. This device consists of a large polycrystalline diamond disc, which is fabricated by the chemical vapor deposition (CVD) technique. Fast neutrons incident on the detector cause  $^{12}\text{C}(n, \text{elastic})$ ,  $^{12}\text{C}(n, n'\gamma)$ , and  $^{12}\text{C}(n, n')3\alpha$  reactions in the diamond and excite hole-electron pairs. The charge from these pairs is extracted through ohmic contact electrodes. The advantages of a CVD diamond detector are follows: (1) Low noise even at room temperature due to its wide band gap  $\sim 5.5\text{eV}$ , (2) Fast time response ( $\sim$  few hundred ps) due to the short lifetimes of the carriers, (3) Radiation hardness due to its strong bonding high-density lattice. Due to its fast time response, a neutron time-of-flight system with a CVD diamond detector can be operated with a short flight path. Thus the detector can complete the TOF measurement before the primary neutrons hit the chamber walls and

before the neutron-induced background increases. We have fabricated the CVD diamond detector (using 1-mm thick 10-mm diameter Type-IIa wafer) and performed preliminary tests at the Omega laser fusion facility<sup>12</sup>. The detector shows a clear response to 14 MeV neutrons. A detailed impulse response for neutrons and the detection efficiency at 4-10 MeV are being investigated.

#### 4.1.2. Lithium Glass SCIFI detector

Counting scattered DD primary neutrons is an alternative method for measuring the areal density of a D<sub>2</sub> filled capsule. We are developing a novel lithium-glass scintillation fiber detector for scattered primary neutron detection<sup>13</sup>. Since the scattered neutrons arrive at a detector after the primary neutrons, the detector needs a huge dynamic range ( $> 10^4$ ) and enough signal-output for low energy neutrons (down to 272 keV). A lithium glass scintillation fiber (LG-SCIFI) is expected to serve this purpose. The LG-SCIFI is an optical fiber faceplate made of lithium scintillation glass. The detector will be located 6m away from the target. Since each neutron is detected using the exothermic reaction  ${}^6\text{Li}(n,t)\alpha$  with  $Q = 4.8$  MeV, the lithium glass produces a large light output ( $\sim 7500$  photons) for a single neutron. Approximately 3% of the scintillation light ( $\sim 225$  photons/neutron) is guided to the end of a scintillation fiber. The scintillation light is amplified by a gated image intensifier. The gated image intensifier is operated in pulsed mode so that only the signals in the TOF window of the scattered primary neutrons are amplified and recorded by a charge-coupled device. Signals from scattered neutrons are counted as individual events in the gated image. The detector works as a  $10^5$  channel, scintillation detector array. With such a multi-channel counting mode detector array, the number of primary neutron hits for each channel is reduced and the interference due to "after glow" from the primary neutron burst is reduced. Using Monte Carlo simulations, we evaluated the background using a polyethylene collimator reducing the background due to non-target scattering. The next step is a proof of principle experiment using a neutron source.

#### 4.2. Gas Sampling System

Nuclear activation measurements with a gas sampling system could play an important diagnostic role because of its unique features. A layer of the target is doped with a tracer material and its activation products form the residual gas in the target chamber after the implosion. The specific reaction product in the gas sample is analyzed by a mass spectroscopy or the detection of  $\gamma$ -ray activity. The sensitivity for this system is quite high. The minimum detection limits of specific nuclear products are expected to be one in  $10^4$  for mass spectroscopy and 1 in  $10^5$  for a gamma ray counting system. This technique is completely free from the backgrounds due to prompt burst of ionizing radiations from implosion. Although the information obtained is time-integrated, by coupling with a layer-selective tracer-doping technique, the activation technique allows the design of spatially resolved experiments. For example, doping  ${}^{38}\text{Ar}$  initially in the DT gas region of the capsule and detecting  ${}^{37}\text{Ar}$  produced by the  ${}^{38}\text{Ar}(n,2n){}^{37}\text{Ar}$  reaction is planned for measuring the areal density of the hot spot region. On the other hand, doping the  ${}^{79}\text{Br}$  in the shell region of DT filled capsule and detecting the  ${}^{79}\text{Kr}$  produced by  ${}^{79}\text{Br}(d^*,2n){}^{79}\text{Kr}$  via knock on deuterons and  ${}^{79}\text{Br}(p,n){}^{79}\text{Kr}$  via primary DD protons is



being designed to measure pusher areal density. Proof of principle experiments are planned at the OMEGA laser facility at the Laboratory for Laser Engineering in Rochester NY in FY02.

#### 4.3 Penumbra Neutron Imaging

Neutron imaging gives crucial information on compression dynamics and asymmetries of implosions. A penumbral imaging system is being developed by scientists from Commissariat à l'Energie Atomique (CEA) for neutron imaging. Penumbral imaging is conceptually similar to pinhole imaging, except that the aperture is larger than the size of neutron source. The coded image observed at the detector plane is a convolution of the source image with an aperture function. The coded image can be reconverted to a measure of the source image using recently developed deconvolution methods<sup>14</sup>. The advantage of the penumbral system is higher statistical accuracy due to the large solid angle of the aperture. Since the NIF has an exclusion zone of about 1m, the distance from target to aperture  $l_1 > 1\text{m}$  is required. A distance from the aperture to the detector  $l_2 < 25\text{ m}$  is preferable due to the finite size of the building. This results in an imaging system with relatively low magnification  $l_2/l_1 < 25$ . Simulations of the NIF target suggest that the diameter of the neutron image will be less than  $25\text{ }\mu\text{m}$  and to see the asymmetry of the neutron producing implosion, a spatial resolution of at least  $5\text{ }\mu\text{m}$  is required<sup>10</sup>. Therefore, spatial resolution better than  $125\text{ }\mu\text{m}$  is required at the detector plane. Led by scientists of General Atomics, we are collaborating on tests of bubble detectors for high-resolution neutron imaging. The bubble detector is an elastic polymer that contains a freon-like superheated liquid droplet. When a neutron strikes the fluorine or chlorine in the droplet, the droplet vaporizes and grows rapidly to  $50\text{ }\mu\text{m}$  in diameter. The spatial resolution of the detector itself is determined by the bubble formation process and readout technique ( $\sim 30\text{-}\mu\text{m}$  resolution). We performed proof-of-principle experiments on OMEGA. Since the efficiency of the detector is limited to  $10^{-5}$ , the resolution of the decoded image is limited by the statistics of the bubbles. Low yield pre-ignition experiments at NIF will require a liquid bubble chamber that has larger detection efficiency. With a liquid bubble chamber,  $5\text{ }\mu\text{m}$  spatial resolution with a signal to noise ratio of 10 should make measurements possible for neutron yields as low as  $\sim 10^{15}$ .

#### 4.4 Gas Cherenkov Gamma Ray Detector

The time history of nuclear reactions during hot spot formation and fuel burn provides crucial information in diagnosing the performance of ICF implosions designed to ignite. Since the time-of-flight spreading of the primary neutrons traversing the exclusion zone limits the temporal resolution of neutron TOF, the use of 16.7-MeV  $\gamma$ -rays produced by the DT reaction is proposed. To observe the 16.7-MeV  $\gamma$ -ray signal from a DT filled capsule, a gas Cherenkov detector has been fabricated by LANL<sup>15</sup>. The  $\gamma$ -rays produced in the target are converted to relativistic electrons by Compton scattering on a beryllium converter. The relativistic electrons pass through a high-pressure  $\text{CO}_2$  gas chamber and produce Cherenkov radiation. The Cherenkov light in the visible and near ultraviolet region is collected by Cassegrain mirror optics and detected by a photo multiplier tube (PMT). Most of the  $\gamma$ -ray backgrounds are produced by  $(n,\gamma)$  reactions (mostly below 10 MeV) in the laser target material. The tunable detection threshold of

the gas Cherenkov system reduces these backgrounds. When the CO<sub>2</sub> pressure is about 2 atmospheres, the Cherenkov radiation in the gas chamber has a steep threshold at 12 MeV. Thus the detector is insensitive to the background  $\gamma$ -ray signal below 12 MeV. The detection response was calibrated using an electron linear accelerator and the expected threshold behavior was confirmed experimentally. The system has been used at OMEGA on a high-yield experiment and a strong  $\gamma$ -ray signal was observed. In this case the time resolution of the system was limited by the time response of the PMT (~250 ps). The PMT has been replaced by a streak camera and integrated tests are underway on an electron linac.

## 5. ACKNOWLEDGMENT

This work was performed under the auspices of the U.S. Department of Energy by the University of California, Lawrence Livermore National Laboratory under contract No. W-7405-Eng-48.

## 6. REFERENCES

1. J. Lindl, Development of the indirect-drive approach to inertial confinement fusion and the target physics basis for ignition and gain, *Phys. Plasmas* **2**, 3933-4024 (1995)
2. H. Brysk, Fusion neutron energies and spectra, *Plasma Phys.* **15**, 611-617, (1973)
3. F. E. Cecil and F. J. Wilkinson, III, Measurement of the ground-state gamma-Ray branching ratio of the *dt* reaction at low energies, *Phys. Rev. Lett.* **53**, 767-770, (1984)
4. D. R. Welch, H. Kislev, and G. H. Miley, Tertiary fusion neutron diagnostic for density-radius product and stability of inertial confinement fusion, *Rev. Sci. Instrum.* **59**, 610-615, (1988); R. D. Petrasso, C. K. Li, M. D. Cable, *et al.*, Measuring implosion symmetry and core conditions in the National Ignition Facility, *Phys. Rev. Lett.* **77**, 2718-2721, (1996); S. Cremer, C. P. Verdon, R. D. Petrasso, Tertiary proton diagnostics in future inertial confinement fusion experiments, *Phys. Plasmas* **5**, 4009-4014, (1998)
5. H. Azechi, M. D. Cable, and R. O. Stapf, Review of secondary and tertiary reactions, and neutron scattering as diagnostic techniques for inertial confinement fusion targets, *Laser Part. Beams* **9**, 119-134, (1991)
6. S. M. Lane, M. D. Cable, W. R. Graves, *et al.*, Advanced Neutron Measurements, Lawrence Livermore National Laboratory Report, No. UCRL-50021-84, 1985, p.5-61
7. J. A. Frenje, K. M. Green, D. G. Hicks, *et al.*, A neutron spectrometer for precise measurements of DT neutrons from 10 to 18 MeV at OMEGA and the National Ignition Facility, *Rev. Sci. Instrum.* **72**, 854-858, (2001)
8. T. E. Blue and D. B. Harris, The ratio of D-T to D-D reactions as a measure of the fuel density-radius product in initially tritium-free inertial confinement fusion-targets, *Nucl. Sci. Eng.* **77**, 463-469 (1981)
9. Stephen P. Hatchett (private communication, Aug. 17, 2000)
10. Thomas J. Murphy, Cris W. Barnes *et al.*, Nuclear diagnostics for the National Ignition facility, *Rev. Sci. Instrum.* **72**, 773-779 (2001)
11. G. J. Schmid, V. Yu. Glebov, A. V. Friesehner, *et al.*, CVD diamond detectors for current mode neutron time-of-flight spectroscopy at OMEGA/NIF, To be published in the Proceedings of the SPIE, vol. 4510A-10 (2001)
12. T. R. Boehly, D. L. Brown, R. S. Craxton, R. L. Keck, *et al.*, Initial performance results of the OMEGA laser system, *Opt. Comm.*, **133**, 495-506 (1997)
13. N. Izumi, R. A. Lerche, T. W. Phillips *et al.*, Development of lower energy neutron spectroscopy for areal density measurement in implosion experiment at NIF and OMEGA, To be published in the Proceedings of the SPIE, vol. 4510A-29 (2001)
14. R. A. Lerche, D. Ress, R. J. Ellis, *et al.*, Neutron penumbral imaging of laser fusion targets, *Laser and Part. Beams* **9**, 99(1991)
15. R. R. Berggren, S. E. Caldwell, J. R. Faulkner, Jr, R. A. Lerche, *et al.*, Gamma-ray based fusion measurements, *Rev. Sci. Instrum.* **72**, 873-876 (2001)